Brigita Tomšič, Maja Blagojević, Nuša Klančar, Erik Makoter, Klara Močenik, Nika Pirš, Sebastijan Šmid, Marija Veskova, Marija Gorjanc, Mateja Kert, Barbara Simončič
University of Ljubljana, Faculty of Natural Sciences and Engineering, Aškerčeva 12, 1000 Ljubljana, Slovenia

Multifunctional Properties of Cotton Fabric Tailored via Green Synthesis of TiO_2/Curcumin Composite

Večfunkcionalne lastnosti bombažne tkanine, pripravljene z zeleno sintezo kompozita TiO_2/kurkumin

***Original scientific article**/Izvirni znanstveni članek*
Received/*Prispelo* 11–2024 • Accepted/*Sprejeto* 1–2025

Corresponding author/*Korespondenčna avtorica:*
Prof. dr. Barbara Simončič
Tel: +38513712557
E-mail: barbara.simoncic@ntf.uni-lj.si
ORCID iD: 00000-0002-6071-8829

Abstract

In this study, a novel green process was developed to produce a multifunctional cotton (CO) fabric incorporating TiO_2/curcumin composites that simultaneously provides UV protection and photocatalytic performance. For this purpose, TiO_2 was synthesised using the sol–gel process; loaded with the natural colourant curcumin as a visible light absorber at two temperatures, i.e., 70 and 350 °C; and applied to the CO fabric via the pad–dry–cure process. For comparison, TiO_2 was synthesised without curcumin under the same conditions. The synthesis conditions at 70 °C ensured the formation of predominantly amorphous TiO_2, while curcumin promoted TiO_2 crystallisation despite the low synthesis temperature. A 350 °C synthesis temperature was high enough to form the polymorphic TiO_2 anatase phase. Although the increase in synthesis temperature and the presence of curcumin in the composites caused a bathochromic shift in light absorption, the photocatalytic activity of all samples was mainly driven by UV light. Chemically modifying the CO fabric significantly reduced the light transmittance of the samples, with the highest absorption of UV light obtained for the sample containing the TiO_2/curcumin composite synthesised at 70 °C. This sample provided excellent UV protection with a UPF value of 51.6. All chemically modified CO samples showed photocatalytic activity, degrading coffee stains and decolourising methylene blue and Rhodamine B dye solutions. The highest photocatalytic efficiency and reusability were obtained again for the CO sample with the TiO_2/curcumin composite synthesised at 70 °C, demonstrating the synergistic effect between TiO_2 and curcumin in the composite prepared under these synthesis conditions.

Keywords: multifunctional cotton, titanium dioxide, *Curcuma longa,* green synthesis

Izvleček

Razvit je bil nov zelen postopek za izdelavo večfunkcionalne bombažne (CO) tkanine z vgrajenimi kompoziti TiO_2/kurkumin, ki hkrati zagotavlja UV-zaščito in fotokatalitsko delovanje. V ta namen je bil sintetiziran TiO_2 s postopkom sol–gel v prisotnosti naravnega barvila kurkumina kot stabilizatorja in absorberja vidne

svetlobe pri dveh temperaturah, in sicer 70 in 350 °C, ter nanesen na CO-tkanino z impregnirnim postopkom. Za primerjavo je bil TiO_2 sintetiziran pri enakih pogojih brez prisotnosti kurkumina. Pogoji sinteze pri 70 °C so omogočili nastanek pretežno amorfnega TiO_2, je pa prisotnost kurkumina podprla kristalizacijo TiO_2 kljub nizki temperaturi sinteze. Temperatura sinteze 350 °C je bila dovolj visoka za tvorbo TiO_2 v polimorfni fazi anatasa. Čeprav sta zvišanje temperature sinteze in prisotnost kurkumina v kompozitih povzročila batokromni premik absorbirane svetlobe, je bila fotokatalitska aktivnost vseh vzorcev pogojena predvsem z UV-svetlobo. Kemijska modifikacija CO-tkanine je bistveno zmanjšala prepustnost svetlobe vseh vzorcev, pri čemer je bila najvišja absorpcija UV-svetlobe dosežena pri vzorcu, ki je vseboval kompozit TiO_2/kurkumin, sintetiziran pri 70 °C. Ta vzorec je zagotovil odlično UV-zaščito z UZF vrednostjo 51,6. Vsi kemijsko modificirani CO-vzorci so bili fotokatalitsko aktivni, kar je privedlo do razgradnje madežev kave in razbarvanja raztopin barvil metilensko modro in Rhodamine B. Največji fotokatalitska učinkovitost in sposobnost ponovne uporabe sta bili tudi v tem primeru doseženi pri CO-vzorcu s kompozitom TiO_2/kurkumin, sintetiziranim pri 70 °C, kar kaže na sinergijski učinek med TiO_2 in kurkuminom v kompozitu, pripravljenim pri teh sinteznih pogojih.
Ključne besede: večfunkcionalni bombaž, titanov dioksid, Curcuma longa, zelena sinteza

1 Introduction

Titanium dioxide (TiO_2) is a wide-band-gap semiconductor that represents one of the most versatile nanomaterials (NMs) in various environmental, energy and biochemical fields owing to its unique properties, including photocatalytic activity; ultraviolet (UV) light absorption; chemical, photochemical and thermal stability; biocompatibility; and non-toxicity [1–3]. In the field of textiles, TiO_2 is an established textile finishing agent, where the application of TiO_2 NMs can impart multifunctional properties such as photocatalytic self-cleaning, UV protection, antimicrobial activity, deodorising properties, hydrophobicity, thermal stability, flame retardancy and electrical conductivity [4]. Furthermore, textiles functionalised with TiO_2 can be advantageously used for smart energy-harvesting textiles and to degrade various pollutants in air or water through a photocatalytic reaction. Regarding the latter, it has been reported that textile substrates can serve as an excellent scaffolding for TiO_2 NMs to enhance their photocatalytic activity [4].

The photocatalytic process in TiO_2 is initiated by irradiation with UV light, enabling the absorption of photons that excite electrons from the valence band (VB) into the conduction band (CB), leaving holes in the valence band. This forms electron–hole pairs that can migrate to the TiO_2 surface and participate in redox reactions in the presence of oxygen and water, forming highly reactive oxygen species (ROS). The latter can react in subsequent reactions with various pollutants, including dye molecules in the water, and cause their degradation [5–7].

The photocatalytic activity of TiO_2 is directly influenced by various factors, including the morphology of NMs and their crystallinity and modifications of the TiO_2 surface and interface [8–11]. It has been reported that nanostructured TiO_2 exhibits better photocatalytic performance compared with bulk materials and that the most effective photocatalytic activity can be obtained for TiO_2 NMs with polymorphic anatase crystal structures owing to their high surface-to-volume ratio and nanoscale crystallite size. Different surface and interfacial engineering strategies for TiO_2 are crucial for improving photocatalytic performance and enhancing visible light photocatalytic activity. These mainly include multiphase heterojunctions, ion doping, metal doping/loading, coupling with other semiconductors and surface sensitisation [10]. As TiO_2 surface sensitisers, synthetic dyes are

usually adsorbed onto the TiO_2 surface to improve its absorption properties for visible light. Such photocatalytic systems are commonly used in dye-sensitised solar cells, with ruthenium-based dyes being the most extensively studied as sensitisers because of their high performance in improving system efficiency. The mechanism of photocatalytic activity for dye-sensitised TiO_2 is based on the dye's absorption of visible light, promoting electron excitation from the highest occupied molecular orbital of the dye (HOMO) to the lowest unoccupied molecular orbital (LUMO), followed by electron transfer from the LUMO with a higher energy level to the CB of the TiO_2 with a lower energy level. This transfer is crucial, as it allows the oxygen reduction reaction to generate superoxide radicals, one of the most important ROS, to take place on the surface of the TiO_2 under visible light [12].

However, synthesising heavy-metal-based dyes is not in line with the principles of green chemistry because of the toxicity and environmental impact of ruthenium [13]. Therefore, replacing ruthenium-based dyes in dye-sensitised TiO_2 composites with non-toxic alternatives is a major research challenge. Following sustainable approaches, natural dyes and pigments derived from natural sources have already been used not only as stabilisers in TiO_2 NM synthesis but also as visible light activators in the construction of dye-sensitised TiO_2 [14–20].

Among the natural colourants, turmeric powder extract, obtained from the *Curcuma longa* plant, has a long tradition in daily life, where it is used as a spice in cooking and as a natural remedy in health and skin care [21–25]. Turmeric powder is also often used as a natural colourant because of its orange-coloured active ingredient, curcumin (diferuloyl methane) [26, 27]. Curcumin contains phenolic hydroxyl and carbonyl groups in its chemical structure that can form attractive hydrogen bonds with TiO_2 [28], contributing to the stability and durability of the composite.

This research aims to develop a new process for the green synthesis of dye-sensitised TiO_2 in the presence of the natural dye curcumin as a visible light absorber and stabiliser and to construct a cotton/TiO_2/curcumin composite with effective multifunctional photocatalytic performance. Cotton fabric was selected as the textile substrate because it is one of the most versatile textile substrates, with a wide range of applications. As a natural fibre with many advantages – such as hydrophilicity, breathability, flexibility, durability and biodegradability - cotton is a very suitable textile substrate for incorporating TiO_2 NMs to produce multifunctional composites for apparel and technical purposes. In addition, cotton can form close bonds with dye-sensitised TiO_2 because of its high functional hydroxyl group content, improving the stability of the composite. In this experiment, two methods were used to synthesise dye-sensitised TiO_2, the first at a temperature of 350 °C, ensuring the formation of the anatase crystal structure of TiO_2, and the second at the more sustainable low temperature of 70 °C, during which the formation of amorphous TiO_2 was expected. We hypothesised that curcumin in the composite would activate the TiO_2 and enhance photocatalytic activity, even when synthesised at lower temperatures. For comparison, TiO_2 was synthesised without curcumin. The effectiveness of the photocatalytic performance of cotton/TiO_2/curcumin composites compared with that of cotton/TiO_2 composites was investigated by determining their UV protection properties and photocatalytic activity.

2 Experimental

2.1 Materials

Chemically bleached 100 % cotton (CO) fabric in plain weave with a mass per unit area of 120 g/m^2 was kindly provided by Tekstina d.o.o., Ajdovščina, Slovenia, for this study. Titanium(IV) isopropoxide (TTIP; ≥ 97.8% concentration), isopropanol (iPrOH; ≥ 99% concentration) and acetic acid (AA; 99% concentration), all products from Sigma Aldrich (USA), were used to prepare TiO_2 nanoparticles (NPs). Turmeric powder (Maestro, Podravka d.d.,

Croatia) was purchased from the local supermarket. Methylene Blue (MB; Sigma Aldrich, USA) and Rhodamine B (RhB; Sigma Aldrich, USA) were used as dyes for monitoring the photocatalytic activity of the samples.

2.2 Synthesis of curcumin-sensitised TiO_2

The curcumin-sensitised TiO_2 synthesis comprised a synthesis of TiO_2 NPs loaded with curcumin. To synthesise TiO_2 NPs, a 4% solution of hydrolysed TTIP in isopropanol and acetic acid was prepared (12 g TTIP in a mixture of 168 g of iPrOH and 20 g of AA). The solution was prepared in a beaker and placed on a magnetic stirrer. While the solution was stirring, 200 g of distilled water was added drop by drop. Afterwards, the sol was left stirring for the next 15 minutes at room temperature to complete the TiO_2 synthesis. The TiO_2 NPs were then filtered and dried at 70 °C. Turmeric extract was prepared in bi-distilled water at a concentration of 5 g/L. Turmeric powder was dispersed into the bi-distilled water at room temperature. The dispersion was boiled for five minutes and then left to cool down for 30 minutes. Afterwards, the dispersion was filtered and dried.

To load TiO_2 NPs with curcumin, a 4 % TiO_2 solution was prepared in 5 g/L of turmeric extract and stirred for 12 hours in the dark at room temperature. The sample was then centrifuged, decanted, rinsed in water three times, and centrifugated and decanted to remove all the unadsorbed curcumin. One half of the sample was then dried at 70 °C for 3 hours and labelled (T+C)70. The other half of the sample amount was additionally calcinated at 350 °C, and that sample was labelled (T+C)350.

For comparison, TiO_2 NPs without curcumin were synthesised under the same conditions at both temperatures, i.e. at 70 °C for the (T)70 sample and at 350 °C for the (T)350 sample.

2.3 Chemical modification of cotton samples

To chemically modify the CO fabric samples, (T)70, (T+C)70, (T)350 and (T+C)350 sols were prepared at 4 % concentration in distilled water and sonicated for 2 hours to obtain homogeneous dispersions. Sols were applied to the CO samples using a pad–dry–cure process, which included fully immersing the CO samples in the sol for 1 minute (four 6 cm × 7 cm CO samples for each sol), squeezing the samples with a 95 ± 2% wet pick-up, drying them at 100 °C for 1 min, and curing them at 150 °C for 5 min. Afterwards, the functionalised CO samples were rinsed with distilled water three times for one minute to remove unbound TiO_2. The synthesis processes for the (T)70, (T+C)70, (T)350 and (T+C)350 powder samples and their application to the CO fabric samples are schematically presented in Figure 1. The sample codes are shown in Table 1 according to the functionalised chemical modification and fabrication of multifunctional cotton samples.

Table 1: Sample codes and description of the cotton chemical modification process

Sample code	Process description
CO(UN)	Untreated cotton sample
CO(T)70	Cotton sample chemically modified with TiO_2 dried at 70 °C
CO(T+C)70	Cotton sample chemically modified with TiO_2/curcumin composite dried at 70 °C
CO(T)350	Cotton sample chemically modified with TiO_2 calcinated at 350 °C
CO(T+C)350	Cotton sample chemically modified with TiO_2/curcumin composite calcinated at 350 °C

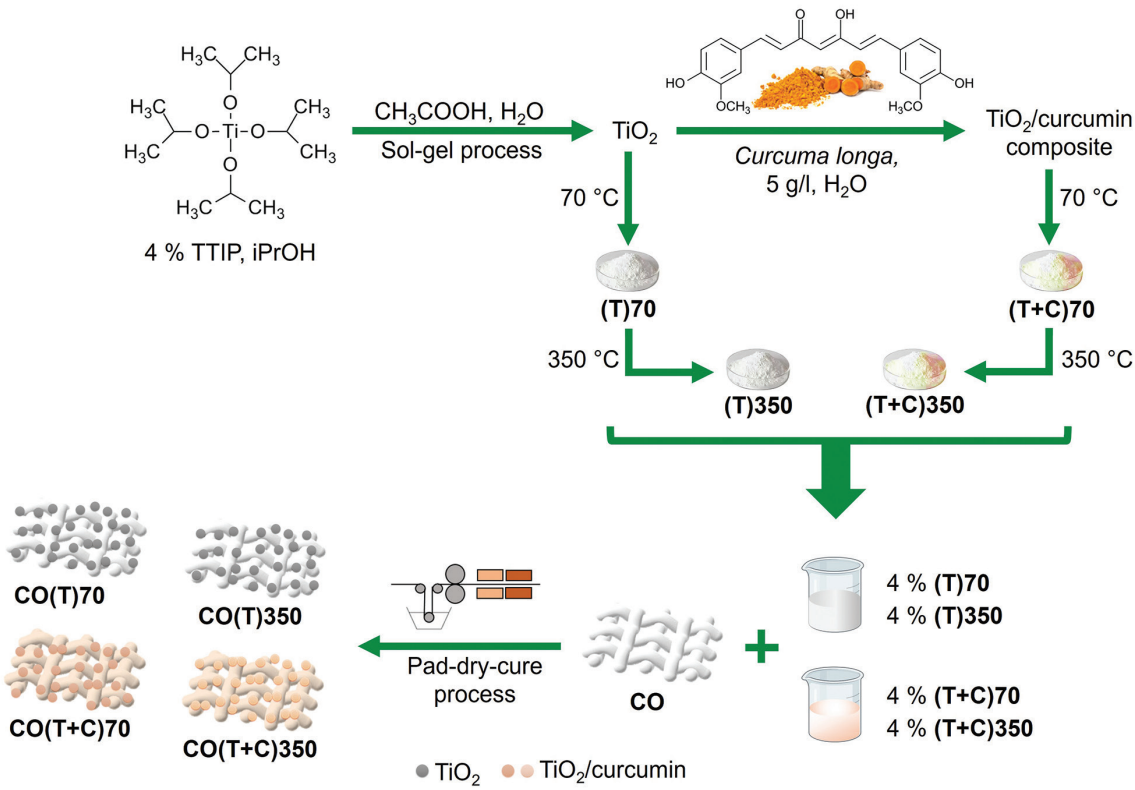

Figure 1: Schematic presentation of the synthesis process for TiO_2 and TiO_2/curcumin composites and the chemical modification of CO samples

2.4 Analysis and Measurement

2.4.1 X-ray diffraction (XRD)

An XRD characterisation was performed for the synthesised (T)70, (T+C)70, (T)350 and (T+C)350 powders, the CO(UN), and the chemically modified CO(T)70, CO(T+C)70, CO(T)350 and CO(T+C)350 samples using a PANalyticalX'Pert PRO X-ray diffractometer (XRD) (CuK α 1 = 1.5406 Å) with a fully open X'Celerator detector (2.1225° 2θ). The XRD pattern was measured from 10 to 90° 2θ with a step size of 0.034° 2θ and a 100 s integration time. The crystallite size, D, of the powder samples was determined from XRD spectra using the Debye–Scherrer equation [29]:

$$D = \frac{0.9\,\lambda}{\beta \cos\theta} \quad (1)$$

where λ is the wavelength of X-rays equal to 0.154 nm; β is the full width at half-maximum (FWHM); and θ is the diffraction angle.

2.4.2 Scanning electron microscopy (SEM) and energy-dispersive X-ray spectroscopy (EDX)

SEM images of the untreated and chemically modified CO samples were acquired using a JSM 6060 LV scanning electron microscope (JEOL, Tokyo, Japan) operated with a primary electron beam accelerated to 10 kV. All samples were coated with a thin layer of gold before examination to provide conductivity and improve the quality of the images.

EDX analysis was performed using a field emission scanning electron microscope, FEG-SEM Thermo Scientific Quattro S (ThermoFischer Scientific, USA). Sample analysis was performed using an Oxford Instruments Ultim Max 65 energy-dispersive detector (EDX) and AZtec software Ver 6.0 (Oxford Instruments, USA). Samples were coated with a thin

carbon layer before analysis to provide conductivity and thus improve the quality of the images.

2.4.3 Inductively coupled plasma-mass spectrometry (ICP-MS)

The Ti concentrations in the CO(T)70, CO(T+C)70, CO(T)350 and CO(T+C)350 samples were determined via ICP-MS using a Perkin Elmer SCIED Elan DRC spectrophotometer. A 0.5 g sample was prepared in a Milestone microwave system via acid decomposition with 65% HNO_3 and 30% H_2O_2. Ti concentrations in studied samples were reported as the mean values of two measurements for each sample. Based on the measured Ti values, the TiO_2 concentration was calculated.

2.4.4 Fourier transform infrared spectroscopy (FTIR)

The chemical compositions was analysed for the synthesised (T)70, (T+C)70, (T)350 and (T+C)350 powder samples, the untreated CO(UN), and the chemically modified CO(T)70, CO(T+C)70, CO(T)350 and CO(T+C)350 samples using an FTIR spectrometer, Spectrum 3 (Perkin Elmer, UK). Spectra between 4000 cm^{-1} and 400 cm^{-1} were recorded with a 4 cm^{-1} resolution and an average of 120 spectra per sample.

2.4.5 UV–Vis spectroscopy

The transmission spectra of the CO(T)70, CO(T+C)70, CO(T)350 and CO(T+C)350 samples were recorded in a wavelength, λ, range of 250–700 nm using a Lambda 850+ UV/Vis spectrophotometer (Perkin Elmer, UK). Three measurements were made for each sample at different warp alignment angles, and the average value of transmittance, T, at each λ was calculated. The average transmission spectra were converted into absorption spectra using the following equation:

$$A = -\log T \tag{2}$$

where A is absorbance. From the absorption spectra, the optical band gap energies, E_g, of the (T)70, (T+C)70, (T)350 and (T+C)350 coatings on the CO samples were determined using the Tauc relation [30, 31]:

$$(\alpha h \nu)^2 = K(h \nu - E_g) \tag{3}$$

where α is the energy-dependent absorption coefficient, equal to 2.303 × A; h is Planck constant; ν is the frequency of the radiation; and K is a constant. According to Planck's radiation law, the energy, E, of radiation is equal to:

$$E = h \nu = \frac{1240}{\lambda} \tag{4}$$

The values of E_g are obtained through extrapolation to $\alpha = 0$ [31].

2.4.6 UV protection

The UV protection of the CO(UN), CO(T)70, CO(T+C)70, CO(T)350 and CO(T+C)350 samples was determined according to Standard EN 13758-1: 2001. Transmission was calculated at three different wavelength ranges, i.e., UVA from 315 to 400 nm and UVB from 290 to 315 nm. The UV protection factor (UPF) was calculated with the following equation [32]:

$$\mathrm{UPF} = \frac{\sum_{290}^{400} E(\lambda) \times \varepsilon(\lambda) \times \Delta\lambda}{\sum_{290}^{400} E(\lambda) \times \varepsilon(\lambda) \times T(\lambda) \times \Delta\lambda} \tag{5}$$

where $E(\lambda)$ represents the solar spectral irradiance; $\varepsilon(\lambda)$ represents the relative erythemal effectiveness; $\Delta(\lambda)$ represents the wavelength interval; and $T(\lambda)$ is the spectral transmittance at the wavelength, λ.

The UPF rating and protection categories were determined using UPF values with the Australian/New Zealand Standard for Sun-Protective Clothing—Evaluation and Classification (AS/NZS 4399, 2020), where UPF values of 15 are suited to the "minimum protection" category; UPF values of 30 are suited to the "good protection" category; and UPF values of 50 are suited to the "excellent protection" category.

2.4.7 Photocatalytic activity

The photocatalytic activity of the CO(T)70, CO(T+C)70, CO(T)350 and CO(T+C)350 samples was determined based on photocatalytic self-cleaning and photocatalytic dye degradation in the solution. To study the photocatalytic self-cleaning performance, the samples were immersed in decanted Turkish coffee (5 g of ground coffee/100 mL water) for 30 s and then air dried and illuminated in a Xenon Alpha instrument (Atlas, USA) at 35 °C and 70% humidity for 4 and 24 hours. Before and after the illumination, the colour coordinates L^*, a^* and b^* in the CIELAB colour space were determined for the samples using a Datacolor Spectro 1050 spectrophotometer (Datacolor, USA). Measurements were performed with a 9 mm aperture under D_{65} illumination and an observation angle of 10°. Ten measurements were performed for each sample, and the colour difference, ΔE^*_{ab}, was calculated using the following equation [33]:

$$\Delta E^*_{ab} = \sqrt{(\Delta L^*)^2 + (\Delta a^*)^2 + (\Delta b^*)^2} \quad (6)$$

where ΔL^*, Δa^* and Δb^* are the differences between the lightness, green–red and blue–yellow colour coordinates, respectively, calculated between the illuminated and nonilluminated samples.

For photocatalytic dye degradation, 0.01 mM MB and 0.02 mM RhB dyes were prepared in distilled water. The CO samples (3.5 cm × 0.8 cm) were immersed in the dye solution (3 ml) that the cuvettes were previously filled with (2 parallels for each sample) and stabilised in the dark for 30 minutes. Two additional cuvettes with only the dye solution were used as a reference (blank). Afterwards, the cuvettes were illuminated for a set period in a Xenotest Alpha instrument equipped with a visible xenon arc lamp (radiation attitude, 0.8–2.5 kVA, and extended radiation range, 300–400 nm). After each illumination period, the absorption spectrum of the dye solution was recorded, from which the maximal value of A at a suitable wavelength was determined (for RhB at 552.9 nm, MB at 664.0 nm) and the corresponding dye concentration in solution was determined using previously prepared calibration curves. The measurements were performed using a Lamda 850+ UV–Vis spectrophotometer (Perkin Elmer, United Kingdom). The photocatalytic degradation efficiency of the RhB and MB dyes was determined based on the dye concentration ratio, C_t/C_0, where C_t is the dye concentration at a given time of illumination, and C_0 is the initial concentration of the dye solution after the adsorption–desorption equilibrium was established [34]. The lower the C_t/C_0 ratio, the higher the degree of dye degradation. From these results, the apparent rate constant, K_{app}, of the photocatalytic reaction was calculated as a measure of the dyes' photocatalytic degradation efficiency, where pseudo-first-order kinetics was used as follow [34]:

$$\ln\frac{C_t}{C_0} = -K_{app}\, t \quad (7)$$

where t is the illumination time. In the case of RhB dye solution degradation, the reusability of the CO samples was determined after 4 repetitive operation cycles.

3 Results and discussion

3.1 Morphological, chemical and optical properties

The morphological, chemical and optical properties of synthesised powder particles and chemically modified CO samples were analysed using XRD, SEM, EDX, ICP-MS, FTIR and UV–Vis spectroscopy. The XRD patterns of the TiO_2 powder samples (Figure 2a) show that the peaks of the (T)350 and (T+C)350 samples were much more intense than those of the (T)70 and (T+C)70 samples. Strong diffraction 2θ peaks in the (T)350 and (T+C)350 samples appearing at 25.3°, 37.8°, 47.9°, 54.0°, 55.3° and 62.6° are characteristic TiO_2 peaks in anatase polymorph phase and correspond to tetragonal crystal planes (1 0 1), (0 0 4), (2 0 0), (1 0 5), (2 1 1) and (2 0 4), respectively [35–37]. In the case of the (T)70 powder sample, the un-sharpness and larger width of the low-intensity peaks indicate that TiO_2 formed

a mostly amorphous phase during the synthesis at 70 °C. Curcumin in the preparation of the (T+C)70 powder sample significantly increased the intensity of the peaks in the diffractogram, suggesting that curcumin promotes TiO_2 crystallisation even at low synthesis temperatures and that polymorphically modified anatase was also partly formed in this sample. Cellulose in the chemically modified CO(T)70, CO(T+C)70, CO(T)350 and CO(T+C)350 samples blurred the characteristic TiO_2 peaks because of the intensive 2θ peaks at 15.0°, 16.8°, 22.7° and 34.5°, which correspond to the (1 1 0), (1 1 0), (2 0 0) and (4 0 0) crystallographic planes of the crystalline structure of cellulose, respectively (Figure 2b) [38]. Only the TiO_2 diffraction 2θ peaks at 25.3° can be seen in the CO(T)350 and CO(T+C)350 samples.

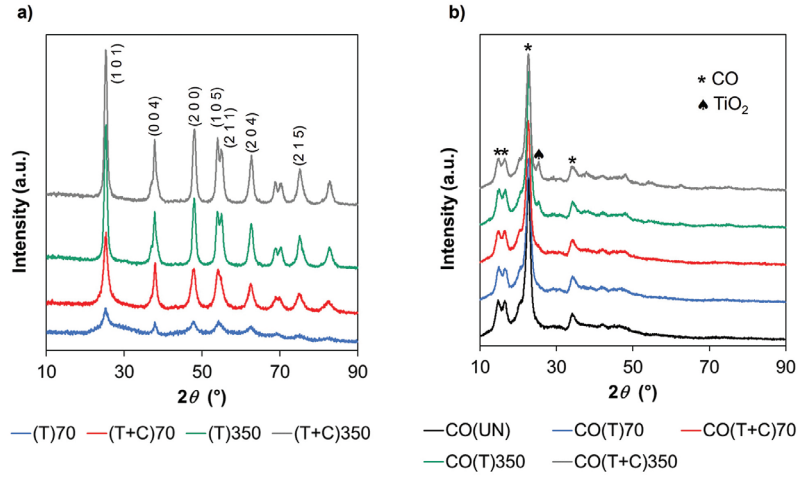

Figure 2: XRD patterns of (T)70, (T+C)70, (T)350 and (T+C)350 powder samples (a) and untreated CO(UN) and chemically modified CO(T)70, CO(T+C)70, CO(T)350 and CO(T+C)350 samples (b)

For the (T+C)70, (T)350 and (T+C)350 powder samples, where the anatase polymorph phase was determined from the XRD patterns, the average crystallite size was calculated using the Debye–Scherrer equation and was on the nanometre scale (Table 2). This indicates that TiO_2 sol–gel synthesis enables the fabrication of NPs of very small sizes, around 10 nm. Similar results have been reported in the literature [39]. The curcumin in the (T+C)350 sample did not significantly influence the crystallite size.

Table 2: Crystallite size of the TiO_2 powder samples calculated using the Scherrer equation

Sample code	2θ (°)	β (rad)	Crystallite size (nm)	Average crystallite size (nm)
(T+C)70	25.3	1.321	4.2	5.6
	47.9	1.468	7.0	
(T)350	25.3	0.876	12.4	11.6
	47.9	0.993	10.7	
(T+C)350	25.3	0.850	12.8	12.4
	47.9	0.954	11.9	

Applying (T)70, (T+C)70, (T)350 and (T+C)350 to the CO samples significantly increased the roughness of the fibre surfaces. Smaller and larger TiO_2 particle agglomerates could be seen at nano- and micro-dimensions (Figure 3a). Although sol–gel synthesis enables the fabrication of very small TiO_2 NPs, they agglomerated after drying. Sonicating the dispersions for 2 hours before applying them to the CO samples did not sufficiently reduce the agglomerate size. The curcumin in the (T+C)70 and (T+C)350

samples increased the agglomeration tendency, as there were visible, micrometre-sized agglomerates in the CO(T+C)70 and CO(T+C)350 samples. The presence of TiO_2 in all chemically modified samples was confirmed by the EDX spectra (Figure 3b) and element mapping (Figure 3c). The ICP-MS results (Figure 3d) show that the highest amount of TiO_2 was present in the CO(T)350 sample, which was 16000 mg/kg. This value was more than three times higher than that in the CO(T)70 sample (5100 mg/kg), and significantly higher than in the CO(T+C)70 sample (10000 mg/kg) and the CO(T+C)350 sample (13000 mg/kg).

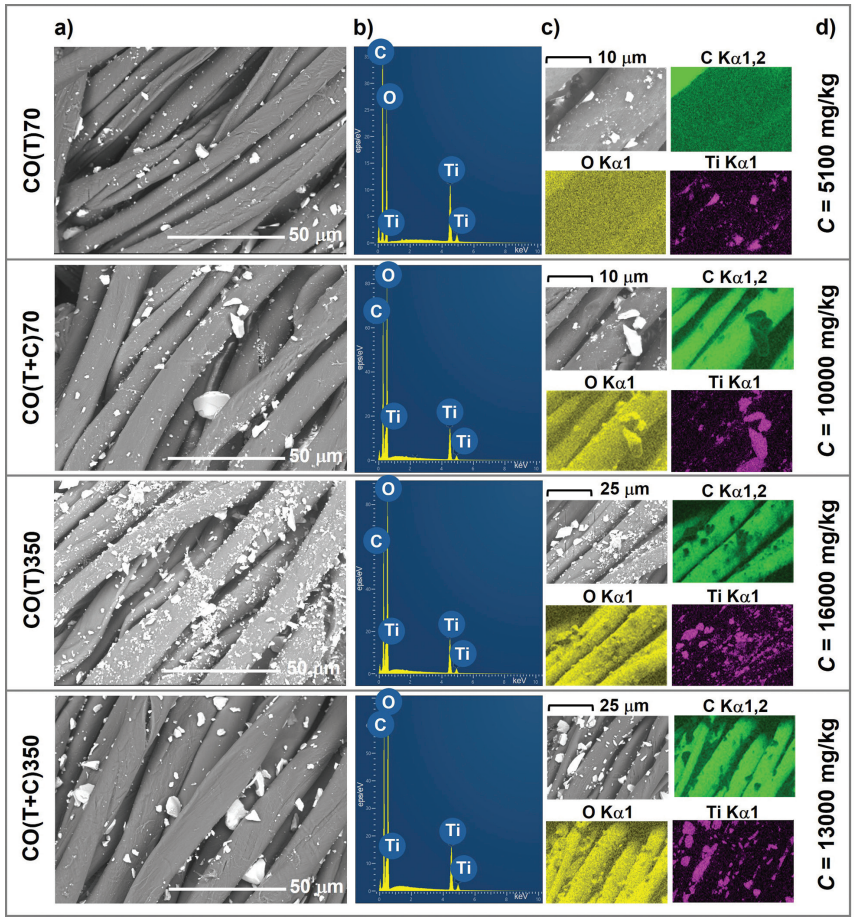

Figure 3: SEM images (a), EDX spectra (b), element mapping images (c) and the TiO_2 concentration determined by ICP-MS (d) of CO(T)70, CO(T+C)70, CO(T)350 and CO(T+C)350 samples

The FTIR spectra of the samples included characteristic absorption bands in the 1500–850 cm^{-1} region, belonging to the cellulose fingerprint [40, 41]. These strong vibrational cellulose bands also blurred the characteristic absorption bands of turmeric in the CO(T+C)70 and CO(T+C)350 samples, appearing in the 1740–1680 cm^{-1} region due to C=O absorption, at 1510 cm^{-1} due to aromatic skeletal stretching vibrations, and at 1030 cm^{-1} due to C–OH stretching vibration [40, 42–44]. The same observation was noticed in our previous study [48]. The TiO_2 anatase absorption bands in the 400–800 cm^{-1} region characterise the stretching vibration modes of different Ti–O bonds (Ti–O–Ti, Ti–O–O, O–Ti–O) (Ti–O–Ti, Ti–O–O, O–Ti–O) [45–47], and could only be observed for the CO(T)350 sample with the highest TiO_2 NP load (see insert in Figure 4).

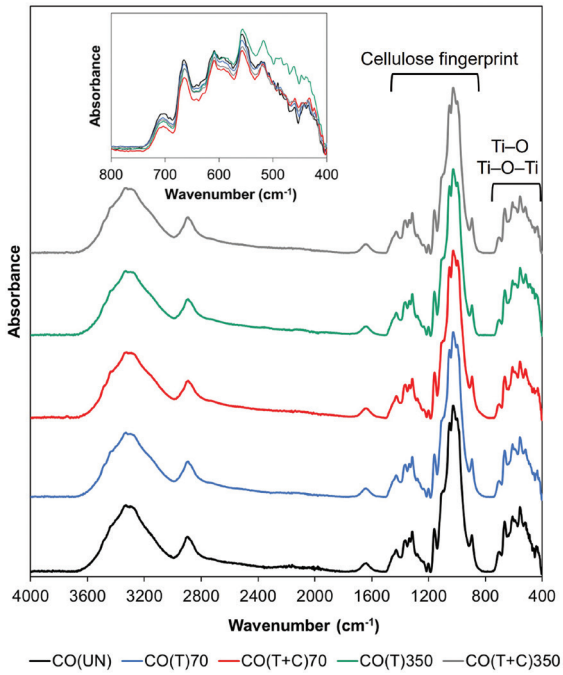

Figure 4: IR ATR spectra of untreated CO(UN) sample and chemically modified CO(T)70, CO(T+C)70, CO(T)350 and CO(T+C)350 samples

The presence of (T)70, (T+C)70, (T)350 and (T+C)350 in the CO samples significantly reduced the transmission of UV radiation through the CO fabric (Figure 5a) owing to increased UV radiation absorption (Figure 5b). The Tauc plots obtained from the absorption spectra (Figure 5c) show that TiO_2 calcination at 350 °C caused a bathochromic shift in the light absorption of TiO_2, as expected, since the value of E_g decreased from 3.41 for CO(T)70 to 3.18 for CO(T)350 (Figure 5d). The presence of curcumin in the TiO_2 composites also slightly decreased the E_g values of the CO(T+C)70 and CO(T+C)350 samples compared with the CO(T)70 and CO(T)350 samples. However, E_g values of 3.30 and 3.16 eV for the CO(T+C)70 and CO(T+C)350 samples correspond to the absorbance values at 376 and 393 nm, respectively, lower than that of visible light. This indicates that despite the bathochromic shift in light absorption, the photocatalytic activity of the samples was mainly driven by UV light.

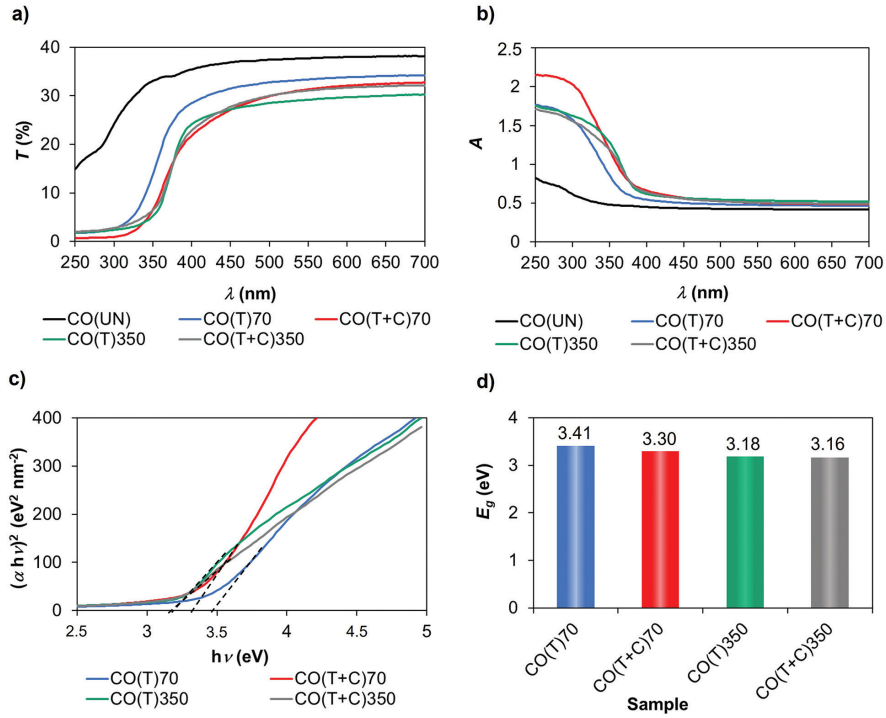

Figure 5: Transmission (a) and absorption (b) spectra of untreated CO(UN) and chemically modified CO(T)70, CO(T+C)70, CO(T)350 and CO(T+C)350 samples; Tauc plots (c) and band gap energy, E_g (d), of CO(T)70, CO(T+C)70, CO(T)350 and CO(T+C)350 samples

3.2 Functional properties

Since TiO_2 has established itself as an effective UV absorber, the UV protection properties of the chemically modified CO samples were determined using the transmission spectra in the 280–400 nm range (Figure 5a). Cotton alone does not offer sufficient protection against UV radiation, which is reflected in a very low UPF value (Table 3). All the chemically modified CO samples retained a higher UVA and UVB blocking effect, increasing the UPF values. Accordingly, the CO(T)70 and CO(T+C)350 samples have minimal UV protection, CO(T)350 has good UV protection and CO(T+C)70 has excellent UV protection. The results also show that increased TiO_2 concentration from 5100 mg/kg for the CO(T)70 sample to 16000 mg/kg for the CO(T)350 sample increased the UPF value from 22.2 to 32.1. These results were expected, as according to our previous studies, both amorphous and crystalline TiO_2 exhibit UV protection properties that do not exceed UPF values of 35 irrespective of the application procedure or concentration [48, 49].

Table 3: UVA and UVB blocking, ultraviolet protection factor (UPF) and the protection categories for the untreated and chemically modified cotton samples

Sample code	UVA blocking (%)	UVB blocking (%)	UPF	Protection category [a)]
CO(UN)	67.1	75.4	3.7	I
CO(T)70	83.0	97.2	22.2	M
CO(T+C)70	89.6	99.0	51.6	E
CO(T)350	89.5	97.6	32.1	G
CO(T+C)350	89.1	97.2	27.3	M

[a)] I – insufficient, M – minimum protection, G – good protection, E – excellent protection

The excellent UV protection factor of the CO(T+C)70 sample with a significantly lower TiO_2 amount than in the CO(T)350 sample was a surprise, as we had found that the curcumin dye alone at the concentration used in our experiment could not provide UV protection for the CO sample with a UPF of 8.75 [48]. The UV protection properties of CO(T+C)70 sample were also higher than those of the CO(T+C)350 sample, which contained TiO_2 in the (T+C) composite in an even higher concentration. However, the absorption spectra (Figure 5b) show that the absorption in the UVB range was significantly higher for the CO(T+C)70 sample than the other samples, blocking 99.0% of UVB radiation, giving a UPF of 51.6 (Table 3). These results indicate that the synergistic effect of TiO_2 and curcumin is undoubtedly achieved in the (T+C)70 composite, which is not the case for the (T+C)350 composite.

The photocatalytic self-cleaning performance of the chemically modified CO samples degraded the coffee stain, which faded and changed colour when illuminated (Figure 6a, b). The results show that the CO(UN) sample had no self-cleaning properties, as the colour of the coffee stain did not fade during illumination but instead became slightly darker (Figure 6b). The colour difference between the non-illuminated CO(T+C)70 and CO(T+C)350 samples stained with coffee and the same stained samples illuminated for 4 and 24 hours was greater than that between the CO(T)70 and CO(T)350 samples, suggesting that the curcumin in the (T+C) composites enhanced the photocatalytic self-cleaning activity of the samples. When the colour coordinates of the chemically modified samples were examined after 24 h of illumination, it was found that the colour of the coffee stain became lighter, greener and bluer than the non-illuminated samples. A comparison of the CO(T+C)70 and CO(T+C)350 samples also shows that the photocatalytic self-cleaning performance of the CO(T+C)70 sample was much more effective than that of the CO(T+C)350 sample, with the greatest differences in the values of ΔE^*_{ab} and the colour

coordinates ΔL^*, Δa^* and Δb^* between the non-illuminated and the coffee stained samples illuminated for 24 hours.

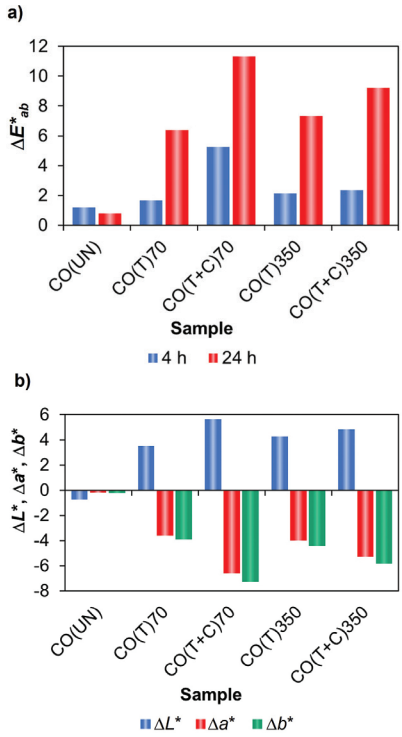

Figure 6: Colour difference, ΔE^*_{ab}, between the unilluminated samples stained by coffee and the stained samples illuminated for 4 and 24 hours (a); difference in colour coordinates, ΔL^*, Δa^* and Δb^*, between the unilluminated samples stained by coffee and the stained samples illuminated for 24 hours (b)

The results for the photocatalytic degradation of the MB and RhB dye solutions show that the photocatalytic degradation efficiency of the investigated dyes was influenced not only by the chemical modification of the CO samples but also by the chemical structure of the dyes (Figure 7 a–e). It should be emphasised that higher dye degradation is associated with a lower C_t/C_0 ratio at a given illumination time. In the case of the MB dye, all tested CO samples showed very similar dye decolourisation kinetics, regardless of their chemical modification (Figure 7a, b). It is also evident that the photostability of the MB dye is very low, as it degraded under illumination even without photocatalytically active CO samples (blank curve in Figure 7a).

When the MB dye was replaced by the RhB dye with significantly higher photostability (blank curve in Figure 7c), the photocatalytic efficiency of the analysed CO samples differed considerably (Figure 7c, d). As expected, the CO(UN) sample showed no photocatalytic activity, but the chemically modified CO samples decolourised the RhB dye solution with the following increased photocatalytic efficiency: CO(T)70 < CO(T)350 < CO(T+C)350 < CO(T+C)70. Accordingly, the curcumin in the TiO_2 composite undoubtedly increased the rate of photocatalytic dye degradation. However, the rate of dye decolourisation in the CO(T+C)70 sample was significantly higher than in the CO(T+C)350 sample, which can be seen in the digital images of the cuvettes filled with RhB solution after 180 minutes of illumination (Figure 7e). This also confirms the findings from the literature [50] that the RhB dye exhibits a strong sensitivity to photocatalytic decolourisation, even with visible light.

To determine the reusability of the photocatalytic performance, one of the most important properties from a technological point of view, the chemically modified CO samples were tested in four consecutive 180-minute cycles of RhB dye solution photodegradation. After each cycle, the degree of dye decolourisation was determined (Figure 7f). The results show that the combination of curcumin and TiO_2 again improved the reusability of the tested CO samples, with the highest photostability achieved for the CO(T+C)70 sample, resulting in 98% decolourisation for the RhB dye after the fourth cycle.

The low photocatalytic activity of the CO(T+C)350 sample compared with the CO(T+C)70 sample was somewhat surprising, as according to the literature, nanocrystalline TiO_2 has higher photocatalytic activity than amorphous TiO_2 [4]. This phenomenon was also confirmed by the higher photocatalytic activity of the CO(T)350 samples compared to the CO(T)70 sample. Therefore, the FTIR spectra of the powder samples were analysed to

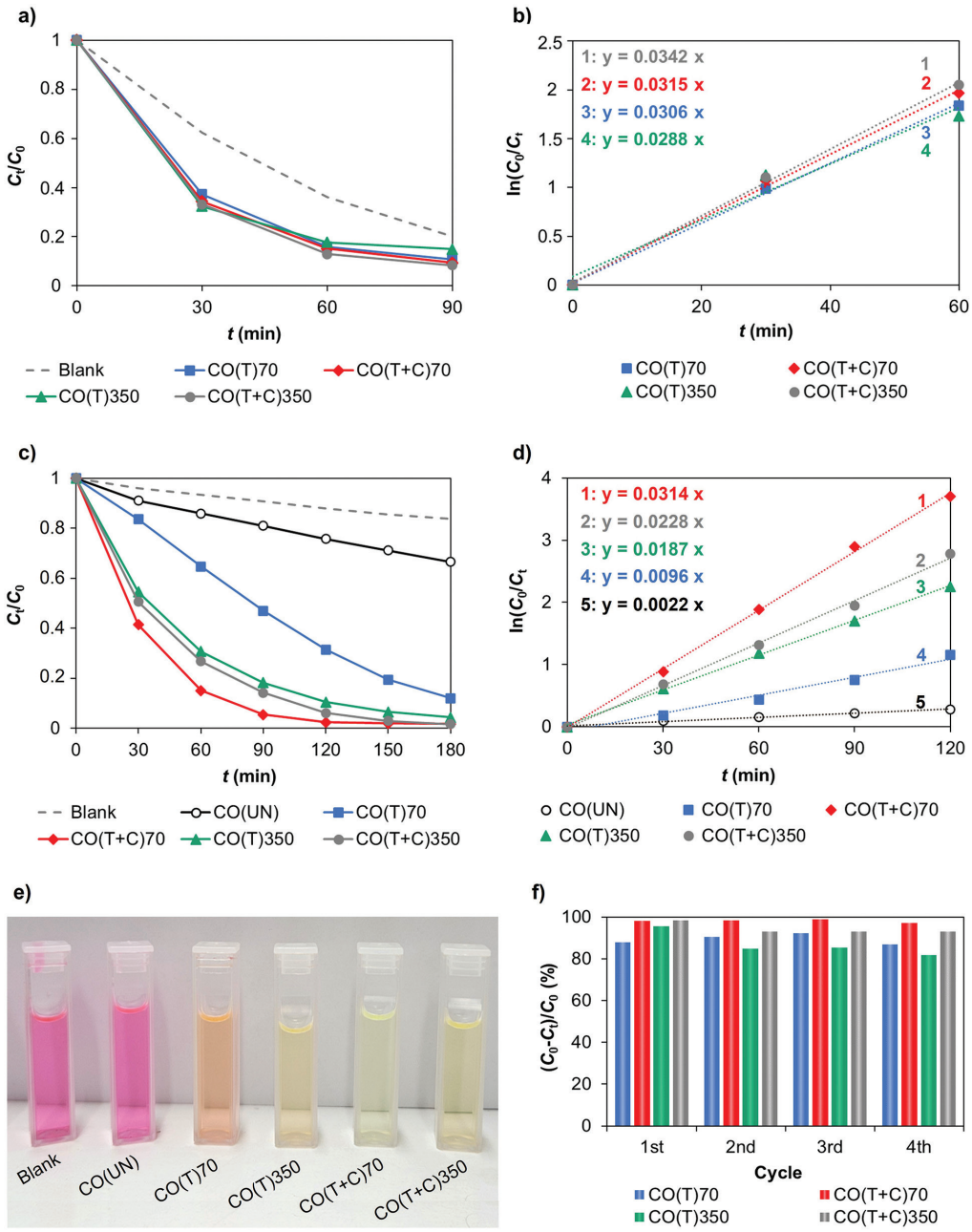

Figure 7: Photocatalytic degradation of MB dye solution without and in the presence of CO samples after different illumination times, t (a); photodegradation kinetics of MB dye solution in the presence of chemically modified CO samples (b); photocatalytic degradation of RhB dye solution without (blank) and in the presence of CO samples after a different illumination time, t (c); photodegradation kinetics of RhB dye solution in the presence of CO samples (d); digital images of cuvettes filled with RhB solution after 180 minutes of illumination without and in the presence of CO samples (e); consecutive 180 min cycles of RhB dye solution photodegradation in the presence of chemically modified CO samples (f)

clarify the chemical changes between the composites (Figure 8). The results show that the (T+C)70 powder sample exhibited characteristic curcumin bands at 1597 cm^{-1} and 1509 cm^{-1} owing to C=C stretching vibrations in the conjugated aromatic system of the curcumin and at 900 cm^{-1} owing to the out-of-plane bending vibrations of aromatic C–H bonds [42–44]. These bending vibrations were not clearly visible in the (T+C)350 powder sample. Furthermore, an additional band in the (T+C)350 powder sample at 1230 cm^{-1}—corresponding to aromatic C–H bending in smaller aromatic fragments such as vanillin or ferulic acid [51]—suggests that the curcumin was partially thermally degraded during the calcination of the composite at 350 °C, which was also accompanied by a slight lightening of the composite colour. This could be why only an additive effect between curcumin and TiO_2 in the (T+C)350 composite was achieved, in contrast to the synergistic effect of the two components in the (T+C)70 composite.

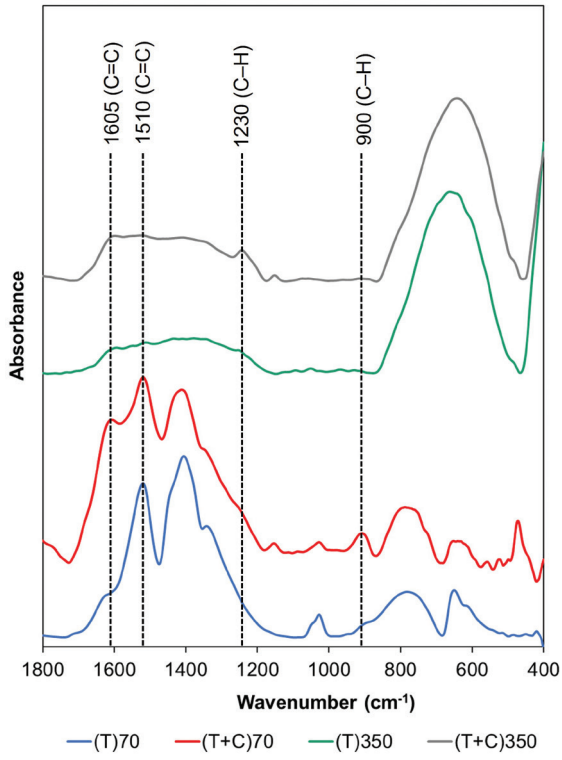

Figure 8: IR ATR spectra of the (T)70, (T+C)70, (T)350 and (T+C)350 powder samples.

4 Conclusion

To summarise, novel multifunctional hybrid CO/TiO_2/curcumin composites with UV protection and photocatalytic self-cleaning performance were successfully prepared according to the principles of green chemistry. XRD analysis showed that the TiO_2 in the powdered (T)350 and (T+C)350 samples was present in the polymorphic anatase phase, while the TiO_2 in the powdered (T)70 sample was amorphous. Curcumin in the (T+C)70 sample significantly promoted the crystallisation of TiO_2, partially converting the amorphous phase into the anatase phase. The crystallite size of the (T)350, (T+C)350 and (T+C)70 powdered samples was less than 13 nm. However, SEM analysis revealed that applying all the powdered samples to the CO fabric resulted in the formation of smaller and larger agglomerates. Increasing the synthesis temperature from 70 to 350 °C and introducing curcumin into the (T+C) composites decreased the E_g values and consequently shifted the absorbance to longer wavelengths. Since the latter did not exceed 400 nm in any sample, it is reasonable to assume that all samples mainly absorb UV light.

The absorption in the UVA and UVB range showed minimal UV protection for the CO(T)70 and CO(T+C)350 samples with UPF values of 22.2 and 27.3, respectively; good UV protection for the CO(T)350 sample with a UPF value of 32.1; and excellent UV protection for the CO(T+C)70 sample with a UPF value of 51.6. Regarding the UPF values, TiO_2 and curcumin had a synergistic effect in the CO(T+C)70 sample, as the UV-blocking effect was more efficient than the additive effect of the CO(T)70 sample and the CO sample coloured only with curcumin at the same concentration.

The analysis of photocatalytic self-cleaning performance based on the degradation rate of coffee stains showed that all chemically modified CO samples caused colour fading, with the highest efficiency obtained for the CO(T+C)70 sample. This showed the largest differences in ΔE^* values between the

non-illuminated and the 24-hour illuminated coffee-stained samples. Examining the photocatalytic degradation of the RhB dye solutions in the presence of the chemically modified CO samples revealed that the CO(T+C)70 sample was the most efficient, followed by the CO(T+C)350 and CO(T)350 samples, and that the lowest efficiency was obtained for the CO(T)70 sample. This confirms that the presence of curcumin in a composite with TiO_2 significantly increases photocatalytic activity, which also applies to the reusability of samples. The low photocatalytic activity of the CO(T+C)350 sample compared with the CO(T+C)70 sample was attributed to the partial thermal degradation of curcumin during the calcination of the (T+C)350 composite at 350 °C, which was confirmed by FTIR analysis.

Summarising the aspects of its composite production and functional properties, the CO(T+C)70 sample can be classified as a green textile-based composite produced via a low-temperature TiO_2 synthesis process in the presence of curcumin, exhibiting excellent multifunctional UV-blocking and recyclable photocatalytic performance. This composite has great application potential in areas such as protective and outdoor textiles, water purification systems, automotive and interior textiles, reusable food packaging.

Author contributions: Brigita Tomšič – conceptualization, methodology, investigation, validation, supervision, review and editing; Maja Blagojević, Nuša Klančar, Erik Makoter, Klara Močenik, Nika Pirš, Sebastijan Šmid, Marija Veskova – investigation, visualization, writing, review and editing; Marija Gorjanc and Mateja Kert – conceptualization, methodology, review and editing; Barbara Simončič – conceptualization, methodology, validation, writing original draft, resources and supervision.

Conflict of interest disclosure: The authors have no relevant financial or non-financial interests to disclose.

Acknowledgments

This research was carried out within the framework of the courses on Advanced Finishing Processes and Chemical Functionalisation of Textiles in the Master Study Programme for Textile and Clothing Planning. The research was co-funded by the Slovenian Research and Innovation Agency (Programme P2-0213 Textiles and Ecology, Infrastructural Centre RIC UL-NTF). The authors would like to thank prof. dr. Matej Dolenec for the support in the XPS analysis and prof. dr. Aleš Nagode for the support in the EDS analysis.

References

1. HUMAYUN, M., RAZIQ, F., KHAN, A., LUO, W. Modification strategies of TiO_2 for potential applications in photocatalysis: a critical review. *Green Chemistry Letters and Reviews*, 2018, **11**(2), 86–102, doi: 10.1080/17518253.2018.1440324.
2. NAM, Y., LIM, J.H., KO, K.C., LEE, J.Y. Photocatalytic activity of TiO_2 nanoparticles: a theoretical aspect. *Journal of Materials Chemistry A*, 2019, **7**(23), 13833–13859, doi: 10.1039/C9TA03385H.
3. NOMAN, M.T., ASHRAF, M.A., ALI, A. Synthesis and applications of nano-TiO_2: a review. *Environmental Science and Pollution Research*, 2019, **26**, 3262–3291, doi: 10.1007/s11356-018-3884-z.
4. RASHID, M.M., SIMONČIČ, B., TOMŠIČ, B. Recent advances in TiO_2-functionalized textile surfaces. *Surfaces and Interfaces*, 2021, **22**, 1–33, doi: 10.1016/j.surfin.2020.100890.
5. ETACHERI, V., DI VALENTIN, C., SCHNEIDER, J., BAHNEMANN, D., PILLAI, S.C. Visible-light activation of TiO_2 photocatalysts: advances in theory and experiments. *Journal of Photochemistry and Photobiology C: Photochemistry Reviews*, 2015, **25**, 1–29, doi: 10.1016/j.jphotochemrev.2015.08.003.
6. GIRISH KUMAR, S., KOTESWARA RAO, K.S.R. Comparison of modification strategies towards enhanced charge carrier separation

and photocatalytic degradation activity of metal oxide semiconductors (TiO_2, WO_3 and ZnO). *Applied Surface Science*, 2017, **391**, Part B, 124–148, doi: 10.1016/j.apsusc.2016.07.081.

7. GUO, Q., ZHOU, C., MA, Z., YANG, X. Fundamentals of TiO_2 photocatalysis: concepts, mechanisms, and xhallenges. *Advanced Materials*, 2019, **31**(50), 1–26, doi: 10.1002/adma.201901997.
8. CARP, O., HUISMAN, C.L., RELLER, A. Photoinduced reactivity of titanium dioxide. *Progress in Solid State Chemistry*, 2004, **32**(1–2), 33–177, doi: 10.1016/j.progsolidstchem.2004.08.001.
9. RAHIMI, N., PAX, R.A., MacA. GRAY, E. Review of functional titanium oxides. I: TiO_2 and its modifications. *Progress in Solid State Chemistry*, 2016, **44**(3), 86–105, doi: 10.1016/j.progsolidstchem.2016.07.002.
10. SHEN, R., JIANG, C., XIANG, Q., XIE, J., LI, X. Surface and interface engineering of hierarchical photocatalysts. *Applied Surface Science*, 2019, **471**, 43–87, doi: 10.1016/j.apsusc.2018.11.205.
11. LI, X., WEI, H., SONG, T., LU, H., WANG, X. A review of the photocatalytic degradation of organic pollutants in water by modified TiO_2. *Water Science & Technology*, 2023, **88**(6), 1495–1507, doi: 10.2166/wst.2023.288.
12. GONUGUNTLA, S., KAMESH, R., PAL, U., CHATTERJEE, D. Dye sensitization of TiO_2 relevant to photocatalytic hydrogen generation: current research trends and prospects. *Journal of Photochemistry and Photobiology C: Photochemistry Reviews*, 2023, **57**, 1–28, doi: 10.1016/j.jphotochemrev.2023.100621.
13. TOMAR, N., AGRAWAL, A., DHAKA, S. V., SUROLIA, P.K. Ruthenium complexes based dye-sensitized solar cells: fundamentals and research trends. *Solar Energy*, 2020, **207**, 59–76, doi: 10.1016/j.solener.2020.06.060.
14. KUSHWAHA, R., SRIVASTAVA, P., BAHADUR, L. Natural pigments from plants used as sensitizers for TiO_2 based dye-sensitized solar cells. *Journal of Energy*, 2013, **2013**(1), 1–8, doi: 10.1155/2013/654953.
15. JAAFAR, S.N.H., MINGGU, L.J., ARIFIN, K., KASSIM, M.B. WAN, W.R.D. Natural dyes as TiO_2 sensitizers with membranes for photoelectrochemical water splitting: an overview. *Renewable and Sustainable Energy Reviews*, 2017, **78**, 698–709, doi: 10.1016/j.rser.2017.04.118.
16. DIAZ-URIBE, C., VALLEJO, W., ROMERO, E., VILLAREAL, M., PADILLA, M., HAZBUN, N., MUÑOZ-ACEVEDO, A., SCHOTT, E., ZARATE, X. TiO_2 thin films sensitization with natural dyes extracted from *Bactris guineensis* for photocatalytic applications: experimental and DFT study. *Journal of Saudi Chemical Society*, 2020, **24**(5), 407–416, doi: 10.1016/j.jscs.2020.03.004.
17. GOULART, S., NIEVES, L.J.J., DAL BÓ, A.G., BERNARDIN, A.M. Sensitization of TiO_2 nanoparticles with natural dyes extracts for photocatalytic activity under visible light. *Dyes and Pigments*, 2020, **182**, 1–6, doi: 10.1016/j.dyepig.2020.108654.
18. HAGHIGHATZADEH, A. Comparative analysis on optical and photocatalytic properties of chlorophyll/curcumin-sensitized nanoparticles for phenol degradation. *Bulletin of Materials Science*, 2020, **43**, 1–15, doi: 10.1007/s12034-019-2016-9.
19. VENUMBAKA, M.R., AKKALA, N., DURAISAMY, S., SIGAMANI, S., KUMAR POOLA, P., RAO, D.S., MAREPALLY, B.C. Performance of TiO_2, Cu-TiO_2, and N-TiO_2 nanoparticles sensitization with natural dyes for dye-sensitized solar cells. *Materials Today: Proceedings*, 2022, **49**(7), 2747–2751, doi: 10.1016/j.matpr.2021.09.281.
20. RAHMAWATI, T. Green synthesis of Ag-TiO_2 nanoparticles using turmeric extract and its enhanced photocatalytic activity under visible light. *Colloids and Surfaces A: Physicochemical and Engineering Aspects*, 2023, **665**, 1–14, doi: 10.1016/j.colsurfa.2023.131206.
21. PRIYADARSINI, K.I. The chemistry of curcumin: from extraction to therapeutic agent. *Molecules*, 2014, **19**(12), 20091-20112, doi: 10.3390/molecules191220091.

22. ABD EL-HADY, M.M., FAROUK, A., SAEED, S.E.-S., ZAGHLOUL, S. Antibacterial and UV protection properties of modified cotton fabric using a curcumin/TiO_2 nanocomposite for medical textile applications. *Polymers*, 2021, **13**(22), 1–14, doi: 10.3390/polym13224027.
23. FULORIA, S., MEHTA, J., CHANDEL, A., SEKAR, M., RANI, N.N.I. M, BEGUM, M. Y., SUBRAMANIYAN, V., CHIDAMBARAM, K., THANGAVELU, L., NORDIN, R., WU, Y.S., SATHASIVAM, K.V., LUM, P.T., MEENAKSHI, D.U., KUMARASAMY, V., AZAD, A.K., FULORIA, N.K. A comprehensive review on the therapeutic potential of *Curcuma longa* Linn. in relation to its major active constituent curcumin. *Frontiers in Pharmacology*, 2022, **13**, 1–27, doi: 10.3389/fphar.2022.820806.
24. UROŠEVIĆ, M., NIKOLIĆ, L., GAJIĆ, I., NIKOLIĆ, V., DINIĆ, A., MILJKOVIĆ, V. Curcumin: biological activities and modern pharmaceutical forms. *Antibiotics*, 2022, **11**(2), 1–27, doi: 10.3390/antibiotics11020135.
25. JIKAH, A.N., EDO, G.I. Turmeric (*Curcuma longa*): an insight into its food applications, phytochemistry and pharmacological properties. *Vegetos (An International Journal of Plant Research & Biotechnology)*, 2024, in press, doi: 10.1007/s42535-024-01038-4.
26. PALASKAR, S.S., KALE, R.D., DESHMUKH, R.R. Application of natural yellow (curcumin) dye on silk to impart multifunctional finishing and validation of dyeing process using BBD model. *Color Research & Application*, 2021, **46**(6), 1301–1312, doi: 10.1002/col.22678.
27. SCHMIDT, M., BIERHALZ, A.C.K., DE AGUIAR, C.R.L. Adsorption, kinetic, and thermodynamic studies of natural curcumin dye on cotton and polyamide fabric and the liberation of its active principle. *The Canadian Journal of Chemical Engineering*, 2024, **102**(10), 1–13, doi: 10.1002/cjce.25277.
28. ABOU-GAMRA, Z.M., AHMED, M.A. Synthesis of mesoporous TiO_2-curcumin nanoparticles for photocatalytic degradation of methylene blue dye. *Journal of Photochemistry and Photobiology, B: Biology*, 2016, **160**, 134–141, doi: 10.1016/j.jphotobiol.2016.03.054.
29. BOKUNIAEVA, A.O., VOROKH, A.S. Estimation of particle size using the Debye equation and the Scherrer formula for polyphasic TiO_2 powder. *Journal of Physics: Conference Series*, 2019, **1410**, 1–7, doi: 10.1088/1742-6596/1410/1/012057.
30. REDDY, K.M., MANORAMA, S.V., REDDY, A.R. Bandgap studies on anatase titanium dioxide nanoparticles. *Materials Chemistry and Physics*, 2003, **78**, 239–245.
31. KARKARE, M.M. The Direct transition and not Indirect transition, is more favourable for Band Gap calculation of Anatase TiO_2 nanoparticles. *International Journal of Scientific & Engineering Research*, 2015, **6**(12), 48–53.
32. SIST EN 13758-1:2002. Textiles - Solar UV protective properties - Part 1: Method of test for apparel fabrics. Geneva : International Organization for Standardization, 12 p.
33. BERGER-SCHUNN, A. Practical color measurement: a primer for the beginner, a reminder for the expert. New York : Wiley, 1994, p. 39.
34. SHAFIQUE, M., MAHR, M.S., YASEEN, M., BHATTI, H.N. CQD/TiO_2 nanocomposite photocatalyst for efficient visible light-driven purification of wastewater containing methyl orange dye. *Materials Chemistry and Physics*, 2022, **278**, 1–14, doi: 10.1016/j.matchemphys.2021.125583.
35. WU, F., LI, X., WANG, Z., GUO, H., WU, L., XIONG, X., WANG, X. A novel method to synthesize anatase TiO_2 nanowires as an anode material for lithium-ion batteries. *Journal of Alloys and Compounds*, 2011, **509**(8), 3711–3715, doi: 10.1016/j.jallcom.2010.12.182.
36. DING, L., YANG, S., LIANG, Z., QIAN, X., CHEN, X., CUI, H., TIAN, J. TiO_2 nanobelts with anatase/rutile heterophase junctions for highly efficient photocatalytic overall water splitting. *Journal of Colloid and Interface Science*, 2020, **567**, 181–189, doi: 10.1016/j.jcis.2020.02.014.

37. TORO, R.G., DIAB, M., DE CARO, T., AL-SHEMY, M., ADEL, A., CASCHERA, D. Study of the effect of titanium dioxide hydrosol on the photocatalytic and mechanical properties of paper sheets. *Materials*, 2020, **13**(6), 1–19, doi: 10.3390/ma13061326.
38. ZHAO, H., KWAK, J.H., ZHANG, Z.C., BROWN, H.M., AREY, B.W., HOLLADAY, J.E. Studying cellulose fiber structure by SEM, XRD, NMR and acid hydrolysis. *Carbohydrate Polymers*, 2007, **68**(2), 235–241, doi: 10.1016/j.carbpol.2006.12.013.
39. AHMAD, M.M., MUSHTAQ, S., AL QAHTANI, H.S., SEDKY, A., ALAM, M.W. Investigation of TiO_2 nanoparticles synthesized by sol-gel method for effectual photodegradation, oxidation and reduction reaction. *Crystals*, 2021, **11**(12), 1–16, doi: 10.3390/cryst11121456.
40. SOCRATES, G. *Infrared and Raman Characteristic Group Frequencies: Tables and Charts*. 3rd edition. New York : Wiley, 2004.
41. TOMŠIČ, B., SIMONČIČ, B., VINCE, J., OREL, B., VILČNIK, A., FIR, M., ŠURCA VUK, A., JOVANOVSKI, V. The use of ATR IR spectroscopy in the study of structural changes of the cellulose fibres. *Tekstilec*, 2007, **50**(1–3), 3–15.
42. ROHMAN, A., DEVI, S., RAMADHANI, D., NUGROHO, A. Analysis of curcumin in *Curcuma longa* and *Curcuma xanthorriza* using FTIR spectroscopy and chemometrics. *Research Journal of Medicinal Plant*, 2015, **9**(4), 179–186, doi: 10.3923/RJMP.2015.179.186.
43. SHARMA, S., DHALSAMANT, K., TRIPATHY, P.P., MANEPALLY, R.K. Quality analysis and drying characteristics of turmeric (*Curcuma longa* L.) dried by hot air and direct solar dryers. *LWT*, 2021, **138**, 1–10, doi: 10.1016/j.lwt.2020.110687.
44. BALLESTEROS, J.I., LIM, L.H.V., LAMORENA, R.B. The feasibility of using ATR-FTIR spectroscopy combined with one-class support vector machine in screening turmeric powders. *Vibrational Spectroscopy*, 2024, **130**, 1–7, doi: 10.1016/j.vibspec.2023.103646.
45. LEÓN, A., REUQUEN, P., GARÍN, C., SEGURA, R., VARGAS, P., ZAPATA, P., ORIHUELA, P.A. FTIR and raman characterization of TiO_2 nanoparticles coated with polyethylene glycol as carrier for 2-methoxyestradiol. *Applied Sciences*, 2017, **7**(1), 1–9, doi: 10.3390/app7010049.
46. RASHID, M.M., ZORC, M., SIMONČIČ, B., JERMAN, I., TOMŠIČ, B. In-situ functionalization of cotton fabric by TiO_2: the influence of application routes. *Catalysts*, 2022, **12**(11), 1–17, doi: 10.3390/catal12111330.
47. GUETNI, I., BELAICHE, M., FERDI, C.A., OULHAKEM, O., ALAOUI, K.B., ZAOUI, F., BAHIJE, L. Novel modified nanophotocatalysts of TiO_2 nanoparticles and TiO_2/Alginate beads with lanthanides [La, Sm, Y] to degrade the Azo dye Orange G under UV-VIS radiation. *Materials Science in Semiconductor Processing*, 2024, **174**, 1–19, doi: 10.1016/j.mssp.2024.108193.
48. TOMŠIČ, B., SAVNIK, N., SHAPKOVA, E., CIMPERMAN, L., ŠOBA, L., GORJANC, M., SIMONČIČ, B. Green in-situ synthesis of TiO_2 in combination with *Curcuma longa* for the tailoring of multifunctional cotton fabric. *Tekstilec*, 2023, **66**(4), 321–338, doi: 10.14502/tekstilec.66.2023075.
49. IVANUŠA, M., KUMER, B., PETROVČIČ, E., ŠTULAR, D., ZORC, M., JERMAN, I., GORJANC, M., TOMŠIČ, B., SIMONČIČ, B. Eco-friendly approach to produce durable multifunctional cotton fibres using TiO_2, ZnO and Ag NPs. *Nanomaterials*, 2022, **12**(8), 1–21, doi: 10.3390/nano12183140.
50. BÖTTCHER, H., MAHLTIG, B., SARSOUR, J., STEGMAIER, T. Qualitative investigations of the photocatalytic dye destruction by TiO_2-coated polyester fabrics. *Journal of Sol-Gel Science and Technology*, 2010, **55**, 177–185, doi: 10.1007/s10971-010-2230-9.
51. CHUMROENPHAT, T., SOMBOONWATTHANAKUL, I., SAENSOUK, S., SIRIAMORNPUN, S. Changes in curcuminoids and chemical components of turmeric (*Curcuma Longa* l.) under freeze-drying and low-temperature drying methods. *Food Chemistry*, 2021, **339**, 1–9, doi: 10.1016/j.foodchem.2020.128121.